A THEORETICAL STUDY ON THE SUCROSE GAP TECHNIQUE AS APPLIED TO MULTICELLULAR MUSCLE PREPARATIONS

II. Methodical Errors in the Determination of Outward Currents

E. Lammel, *Department of Physiology, Philipps Universität, D-3550 Marburg/Lahn, Federal Republic of Germany*

ABSTRACT This paper presents a mathematical model for analyzing systematic errors associated with the membrane conductance of multicellular muscle preparations as determined in a sucrose gap apparatus. The errors arise because of the interdiffusion of sucrose and saline in the interstitial fluid spaces, which results (*a*) in spatial variations of equilibrium potentials, membrane conductance, and solution conductivity, and (*b*) in the existence of a liquid junction potential. The model was applied to simulate the measurement of outward currents predominantly carried by potassium ions; time variations were not considered. Output current/voltage (I/V) curves were computed and compared with the membrane I/V relationship used in the computation. The output curves look very much like experimental results but are distorted considerably from the membrane I/V relationship: (*a*) under favorable conditions (negligible shunt current), the membrane current is overestimated over the entire range of membrane potential, (*b*) regions with negative slope conductance of I/V relations with "anomalous rectifier" properties are found to be less pronounced or even absent, and (*c*) resting potentials may be either increased or reduced. The origin of these errors is related to currents emerging from the sucrose compartment (local circuit as well as externally applied currents). Their dependence on several experimental parameters is discussed.

INTRODUCTION

In the preceding paper (Lammel, 1981) equations were given that describe concentration distributions established by saline-sucrose interdiffusion in the interstitial fluid spaces of multicellular muscle preparations during sucrose gap experiments. This article is concerned with the interference of such distributions with the measurement of membrane current/voltage (I/V) relations. Interference of this kind must be expected for several reasons. (*1*) The ion concentration profiles extending into the sucrose compartment from either side are important in determining the two fractions of the externally applied current that do not pass membrane areas within the test compartment: (*a*) the fraction flowing extracellularly through the sucrose gap (shunt current), and (*b*) the fraction leaving cells through membrane areas within the sucrose compartment. (*2*) Changes of ion concentrations within the test compartment and adjacent regions of the sucrose compartment are associated with changes of the membrane conductance. (*3*) Ion concentration gradients in the interstitial fluid spaces are related to (*a*) spatial variations of ionic equilibrium potentials and (*b*) the presence of a liquid

junction potential. Both of the latter effects give rise to the flow of local circuit currents that superpose themselves on the currents derived from the external current source. Systematic errors inherent in the sucrose gap method arising from these complications were analyzed by a mathematical model that describes the electrical events occurring in a heart trabecula, taking into account the dependence of several physical variables on ion concentrations. The present investigation is restricted to outward membrane currents carried predominantly by potassium ions. The current-passing properties of the cell membrane were modeled either on the constant field equation (Goldman, 1943; Hodgkin and Katz, 1949) or on a modified equation of this type which accounts for the "anomalous rectification" (Katz, 1949; Hodgkin and Horowicz, 1959; Hutter and Noble, 1960) characteristic for skeletal and cardiac muscle fibers.

GLOSSARY

a	cell diameter (cm)
d	trabecula diameter (cm)
A_c	cross-sectional area of the trabecula (cm^2)
A_{ce}	surface area of cells per unit length of the trabecula (cm)
$c_{j,o}$	interstitial concentration of ion species j (mol/cm^3)
$c_{j,i}$	intracellular concentration of ion species j (mol/cm^3)
$c_{j,R}$	concentration of ion species j in Ringer's solution (mol/cm^3)
$c_{K,o}$; $c_{Na,o}$	interstitial concentrations of potassium and sodium, respectively (mol/cm^3)
$c_{K,i}$; $c_{Na,i}$	intracellular concentrations of potassium and sodium, respectively (mol/cm^3)
$c_{K,R}$; $c_{Na,R}$	concentrations of potassium and sodium, respectively, in Ringer's solution (mol/cm^3)
E_e	liquid junction potential (V)
g_j	membrane chord conductance per unit trabecula length for ion species j ($\Omega^{-1}\ cm^{-1}$)
G_i	conductivity of intracellular fluid medium including the conductivity of nexuses between fibers ($\Omega^{-1}\ cm^{-1}$)
G_R	conductivity of Ringer's solution ($\Omega^{-1}\ cm^{-1}$)
i_e	axial current flowing extracellularly through the trabecula (A)
i_i	axial current flowing intracellularly through the trabecula (A)
i_m	membrane current per unit length of the trabecula (A/cm)
i_K	component of i_m carried by potassium ions (A/cm)
i_{Na}	component of i_m carried by sodium ions (A/cm)
$i_{e,l}$	component of i_e attributed to electromotive forces present in the trabecula (local circuit current) (A)
$i_{e,I}$	component of i_e attributed to external current source (A)
$i_{m,l}$	component of i_m attributed to electromotive forces present in the trabecula (local circuit current) (A/cm)
$i_{m,I}$	component of i_m attributed to external current source (A/cm)
I	total axial current flowing through the trabecula (A)
P_K	potassium permeability coefficient (cm/s)
P_{Na}	sodium permeability coefficient (cm/s)
r_e	extracellular resistance per unit length of trabecula (Ω/cm)
r_i	intracellular resistance per unit length of trabecula (Ω/cm)
r_m	membrane chord resistance referred to unit trabecula length (Ωcm)
R_e	total extracellular resistance across sucrose gap residing in the interstitial fluid spaces (Ω)
R_i	total intracellular resistance across sucrose gap (Ω)
t_j	transport number of ion species j
T	temperature (K)

u_j	mobility of ion species j (cm^2/Vs)
u_K, u_{Na}, u_{Cl}	mobilities of potassium, sodium, and chloride, respectively (cm^2/Vs)
V_e	potential in the interstitial fluid spaces (V)
V_i	potential inside the cells (V)
V_m	transmembrane potential (membrane potential) (V)
V_r	computed resting potential in the test region (V)
V_j	equilibrium potential of ion species j (V)
V_K	equilibrium potential of potassium (V)
$V_{K,Na}$	"mixed" equilibrium potential of potassium and sodium (V)
$V_{m,I}$	membrane potential level related to $i_{m,I}$ (V)
$\Delta V_{m,I}$	membrane potential drop related to $i_{m,I}$ (V)
z	axial coordinate along trabecula (cm)
Z_j	valency of ion species j
ρ	fraction of cross-sectional area of the trabecula not occupied by cells

THEORETICAL MODEL

The model is based on the experimental situation schematically illustrated in Fig. 1, where a heart bundle is shown suspended in three adjacent fluid compartments containing physiological saline (Ringer), sucrose, and potassium chloride solution (all isotonic). Electrical current is applied to the bundle from an external current source via the KCl to the saline compartment, so that a large portion of current flows through the interior of the muscle fibers, the remainder, as shunt current, through the interstitial fluid spaces of the bundle. For mathematical simplicity all heart cells of the bundle are regarded physiologically as behaving like parallel fibers, all cylindrical, and of the same diameter, extending along the whole length of the bundle. (The same model was used in the preceding paper [Lammel, 1981]). Accordingly, the interstitial fluid spaces beneath the endothelium cell sheath (the "endocardium") are assumed to make up a volume of simple geometrical shape, e.g., without any narrow recesses between fibers and occupying the same area in every bundle cross section. The basis of these assumptions and simplifications is as follows: heart cells are connected with each other by low-resistance nexuses which provide electrical continuity between them and endow the bundle with electrical properties approximating those of a linear cable, when external current is applied in the way as indicated in Fig. 1 (Trautwein et al., 1956; Weidmann, 1970; Noble, 1975; Lammel et al., unpublished information). After a bundle has been placed in a sucrose gap apparatus and steady diffusion fluxes of saline and sucrose have been established, there are concentration profiles in the interstitial spaces that

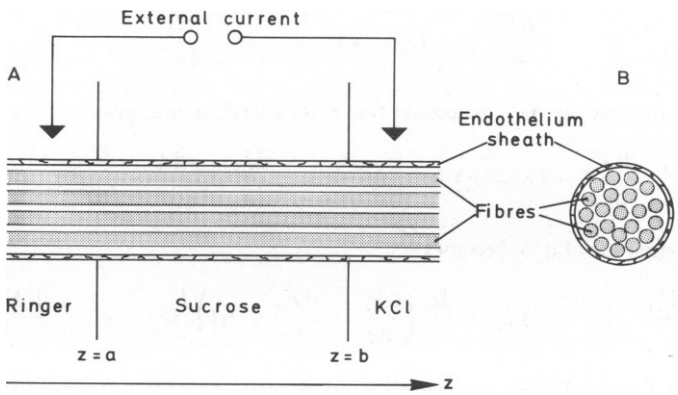

FIGURE 1 Schematic representation of heart trabecula under sucrose gap conditions. *A*, axial section, *B* cross section.

normally extend in the longitudinal and radial direction in relation to the main axis of the bundle. However, the bundles that concern us are thin enough and their surface layer (the endothelium cell sheath) has low permeability, so that radial diffusion gradients become small (see Lammel, 1981; Discussion). Therefore, as a good approximation, we will assume that the extracellular ion concentration in a given cross section is the same for all fibers and will be mathematically described by its average. The advantage of these simplifications is that the problem is thereby reduced to that of a one-dimensional system. As a further simplification, we will not consider changes of the diffusion profiles due to current flow along the model trabecula.

If V_i is the potential of the bundle inside a cell and V_e that in the interstitial fluid space, both at a point z along the main axis of the bundle, then V_m, the transmembrane potential (membrane potentials), is

$$V_m = V_i - V_e. \tag{1}$$

Also, according to the cable properties of the bundle,

$$\frac{dV_i}{dz} = -r_i\, i_i \tag{2}$$

and

$$\frac{dV_e}{dz} = -r_e\, i_e + \frac{dE_e}{dz}, \tag{3}$$

where i_i and i_e are the internal and external components of longitudinal current passing through the bundle, r_i the internal (i.e., the parallel internal resistance of all fibers) and r_e the external resistance, both per unit length, and E_e the liquid junction potential set up by the ionic concentration gradients within the interstitial fluid spaces. Defining I as the total longitudinal current through the bundle and i_m as the membrane current per unit length of trabecula, one has

$$I = i_e + i_i \tag{4}$$

and

$$i_m = -\frac{di_i}{dz} \quad \text{(outward current positive)}. \tag{5}$$

Combining Eqs. 1–5 one obtains

$$\frac{dV_m}{dz} = -(r_e + r_i)\, i_i + r_e I - \frac{dE_e}{dz}. \tag{6}$$

Differentiating Eq. 6, while taking into account that r_e is dependent on z, gives

$$\frac{d^2V_m}{dz^2} = (r_e + r_i)\, i_m - i_i \frac{dr_e}{dz} + r_e \frac{dI}{dz} + I \frac{dr_e}{dz} - \frac{d^2E_e}{dz^2}. \tag{7}$$

This, after combination with Eq. 6, becomes

$$\frac{d^2V_m}{dz^2} = (r_e + r_i)\, i_m + \frac{dr_e}{dz}\left(\frac{dV_m}{dz} + \frac{dE_e}{dz} + r_i I\right)\Big/(r_e + r_i) - \frac{d^2E_e}{dz^2}. \tag{8}$$

The term $r_e dI/dz$ has been omitted, because in the sucrose section $dI/dz = 0$, whereas $r_e = 0$ is assumed in both electrolyte compartments. Because time variations are not considered in the present analysis capacitive currents have been ignored.

The following subsidiary equations which specify the dependence of several variables in Eq. 8 on ion

concentrations and membrane potential were used (*a*) to give electrical properties resembling those of cell membrane and (*b*) to allow for the variation of the ion concentrations along the preparation:

(*1*) i_m in Eq. 8 is the sum of individual ion currents. Only two ions are considered here, Na^+ and K^+. Ca^{2+} and Cl^- are disregarded for simplicity. The cellular concentrations ($c_{Na,i}$ and $c_{K,i}$) are taken to remain unaltered under the conditions analyzed. A case in which a loss of cellular potassium into the interstitial fluid spaces is assumed to occur, however, will be considered in connection with Fig. 8. Two types of current equation are used alternatively: the first type is the constant-field equation (Goldman, 1943; Hodgkin and Katz, 1949; see monotonic current/voltage curves 1-1b in Fig. 2 *B*) which for the potassium and sodium currents has the form:

$$i_K = P_K A_{ce} \frac{V_m F^2}{RT} \frac{c_{K,o} - c_{K,i} \exp(V_m F/RT)}{1 - \exp(V_m F/RT)} \tag{9a}$$

$$i_{Na} = P_{Na} A_{ce} \frac{V_m F^2}{RT} \frac{c_{Na,o} - c_{Na,i} \exp(V_m F/RT)}{1 - \exp(V_m F/RT)}, \tag{9b}$$

where P_K is the potassium and P_{Na} the sodium permeability coefficient. $c_{K,o}$ and $c_{Na,o}$ are the extracellular concentrations of these ions. A_{ce} is the surface area of cells per unit length of the trabecula,

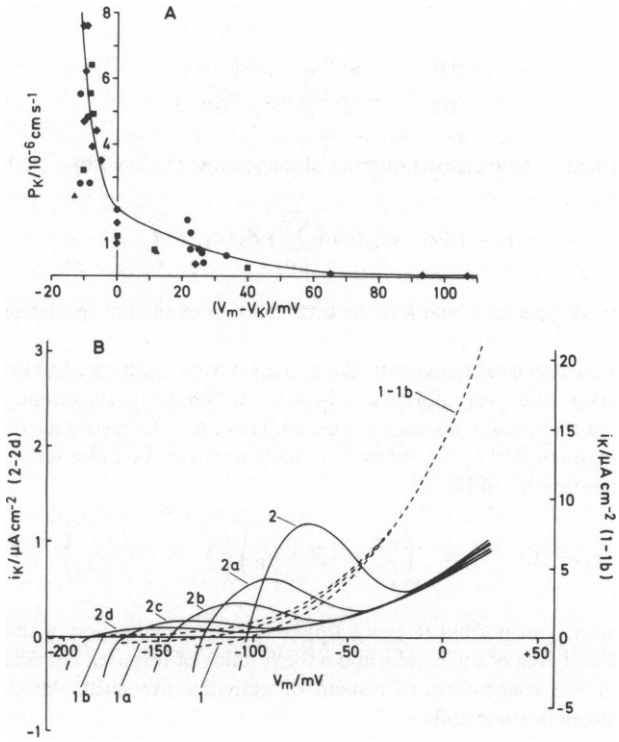

FIGURE 2 (*A*) Empirical relationship expressing the potassium permeability coefficient (P_K) as a function of the driving force ($V_m - V_K$). Symbols represent experimental data at different external concentrations $c_{K,o}$ taken from Hodgkin and Horowicz (1959). In mmol/liter: ♦, $c_{K,o}$ = 95; ▲, $c_{K,o}$ = 50; ■, $c_{K,o}$ = 10; ●, $c_{K,o}$ = 2.5. Curve illustrates Eq. 10 used to fit these data. (*B*) Potassium current/voltage curves representing the constant-field equation; 1-1b: $P_K = 10^{-6}$ cm s^{-1}, $c_{K,o}$ = 2.5, 1.0, 0.1 mmol/liter respectively (right-hand-side ordinate); 2-2d: P_K dependent on driving force according to Eq. 10, $c_{K,o}$ = 2.5, 1.0, 0.5, 0.2, 0.1 mmol/liter respectively (left-hand-side ordinate). Internal potassium concentration: $c_{K,i}$ = 150 mmol/liter.

and F, R, and T have their usual meanings. The second type is a modified constant-field equation in which the potassium conductance shows "anomalous rectification" (Katz, 1949; Hodgkin and Horowicz, 1959; Hutter and Noble, 1960): there is a strongly nonlinear voltage dependence, characteristic for skeletal and cardiac muscle fibers. The definition of P_K, in this case, is by means of an empirical relationship (see Fig. 2 *A*) which can be used to fit the experimental data obtained in frog skeletal muscle by Hodgkin and Horowicz (1959), still the most detailed data of this kind:

$$P_k = \begin{cases} a_0 + a_1(V_m - V_K) + a_2(V_m - V_K)^2 + a_3(V_m - V_K)^3, & V_m - V_K \le 0 \text{ mV} \\ b_0 + b_1(V_m - V_K) + b_2(V_m - V_K)^2 + b_3(V_m - V_K)^3, & 0 \le V_m - V_K \le 90 \text{ mV} \\ c_1/(V_m - V_K + c_2), & V_m - V_K \ge 90 \text{ mV}, \end{cases} \tag{10}$$

where $a_o = b_o = 2.01285 \text{ cm s}^{-1}$, $a_1 = -1.241 \cdot 10^2 \text{ cm s}^{-1} \text{ V}^{-1}$, $a_2 = 1.1 \cdot 10^4 \text{ cm s}^{-1} \text{ V}^{-2}$, $a_3 = -2.014 \cdot 10^6 \text{ cm s}^{-1} \text{ V}^{-3}$, $b_1 = -60.15 \text{ cm s}^{-1} \text{ V}^{-1}$, $b_2 = 6.0795 \cdot 10^2 \text{ cm s}^{-1} \text{ V}^{-2}$, $b_3 = -2.022 \cdot 10^3 \text{ cm s}^{-1} \text{ V}^{-3}$, $c_1 = 2.76597 \cdot 10^{-2} \text{ cm s}^{-1} \text{ V}$, $c_2 = 0.466548$ *V*. V_K represents the potassium equilibrium potential.

Potassium current/voltage relations computed by Eqs. 9a and 10 for different levels of $c_{K,o}$ are illustrated in Fig. 2 *B* (curves 2–2d).

(*2*) The terms for the liquid junction potential in Eq. 8 are related to the external ion concentrations ($c_{j,o}$) by

$$\frac{dE_e}{dz} = -\frac{RT}{F} \sum_{j-1}^{k} \frac{t_j}{Z_j} \frac{d \ln c_{j,o}}{dz}, \tag{11}$$

where Z_j is the valency and t_j the transport number of ion species j defined by

$$t_j = (|Z_j| c_{j,o} u_j) \left(\sum_{i-1}^{k} |Z_i| c_{i,o} u_i \right)^{-1}. \tag{12}$$

u_j is the mobility of the ion species j, and k is the total number of the ion species present (e.g. Kortüm, 1957; p. 257).

(*3*) As already mentioned in connection with Eq. 8, the external resistance (r_e) in both saline and high KCl compartment is taken to be negligible; i.e., $dV_e/dz = 0$. Similarly, the ohmic resistance across the endothelium cell layer of the bundle has been neglected. However, the resistance of the interstitial fluid spaces of the bundle segment within the sucrose compartment can be quite large and is expressed, in terms of local ion concentrations, in Eq. 13

$$r_e = (G_R A_c \rho)^{-1} \left(\sum_{j-1}^{k} u_j |Z_j| c_{j,R} \right) \left(\sum_{j-1}^{k} u_j |Z_j| c_{j,o} \right)^{-1}, \tag{13}$$

where G_R is the conductivity of normal Ringer's fluid, $c_{j,R}$ the concentration of the ion species j in this fluid, A_c the cross-sectional area of the bundle and ρ the fraction of this area not occupied by cells. (Note that in Eqs. 9 and 11 ion concentrations instead of activities are used. Also, changes of u_j with concentration are not taken into account).

After inserting Eqs. 9–13 into 8, solutions were obtained by numerical integration (see below).

For the interpretation of the results it is convenient to consider the currents in the preparation (i_m, i_e, and i_i) as being composite currents consisting of two components (see Fig. 3). One component is derived from the external current source (supplying the current I). The other is a local circuit current caused by the electromotive forces present in the model preparation itself, which are (*a*) the liquid junction potential, E_e, and (*b*) the ionic equilibrium potentials at the membrane. (Essential for the flow of this current is the spatial variation of the equilibrium potentials of which only V_K is represented in Fig. 3). To

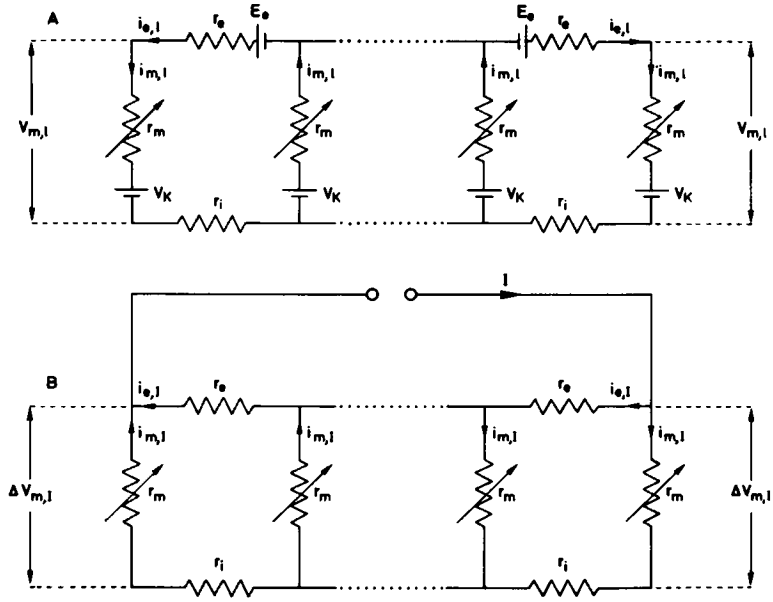

FIGURE 3 Equivalent circuit representing the muscle bundle including membrane resistance r_m, extracellular resistance r_e, and intracellular resistance r_i. (*A*) Flow of local circuit currents ($i_{m,l}$; $i_{e,l}$) results from spatial variation of equilibrium potentials (V_K) and from liquid junction potential (E_e). (*B*) Currents $i_{m,l}$ and $i_{e,l}$ are derived from external current source. Total current in each branch is the sum of the two components.

subdivide a solution of Eq. 8 into these two components, i_m in Eq. 8 was reformulated in terms of Eq. 14:

$$i_m = \sum_j g_j (V_m - V_j), \tag{14}$$

where j again denotes the ion species for which the membrane chord conductance is g_j and the equilibrium potential V_j. (In the present case j is specified as K and Na.)

$$V_j = \frac{RT}{Z_j F} \ln \frac{c_{j,o}}{c_{j,i}}, \tag{15}$$

where $c_{j,o}$ and $c_{j,i}$ are the outside and inside ion concentrations, respectively. The distribution of the membrane potential along the model trabecula [$V_m(z)$ obtained by integration of Eq. 8 for a given set of conditions] is related to a specific distribution of $g_j(z)$ which can be computed from Eqs. 9 and 14. Taking this distribution we put

$$i_{m,l} = \sum_j g_j \Delta V_{m,l} \tag{16}$$

and

$$i_{m,l} = \sum_j g_j (V_{m,l} - V_j) \tag{17}$$

where

$$i_m = i_{m,I} + i_{m,l} \tag{18}$$

and

$$V_m = V_{m,I} + \Delta V_{m,l}. \tag{19}$$

The suffixes I and l denote the external and local origin of the currents and associated potentials. With these definitions, Eq. 8 can be split into the following two equations:

$$\frac{d^2V_{m,I}}{dz^2} = (r_e + r_i)\sum_j g_j (V_{m,I} - V_j) + \frac{dr_e}{dz}\left(\frac{dV_{m,I}}{dz} + \frac{dE_e}{dz}\right)\Big/(r_e + r_i) - \frac{d^2E_e}{dz^2} \tag{20}$$

$$\frac{d^2\Delta V_{m,l}}{dz^2} = (r_e + r_i)\sum_j g_j \Delta V_{m,l} + \frac{dr_e}{dz}\left(\frac{d\Delta V_{m,l}}{dz} + r_i I\right)\Big/(r_e + r_i), \tag{21}$$

of which Eq. 20 deals exclusively with the effects of the electromotive forces present in the model preparation itself (see Fig. 3 *A*) and Eq. 21 only with those due to current applied from the external current source (Fig. 3 *B*). Particularly, when no current is applied from the external source, $\Delta V_{m,l} = 0$, $V_{m,I} = V_m$ and Eq. 20 is equivalent to Eq. 8.

For the validity of the separation method note that, since the g_j in Eqs. 20 and 21 are known functions only of z [derived from $V_m(z)$ and therefore the same as in Eq. 8], the sum of the solutions of these equations satisfies the original differential Eq. 8, providing the boundary conditions are satisfied appropriately. In practice, g_j values were computed from Eqs. 9 and 14 at the two edges of each integration interval on the basis of a solution of Eq. 8. Using these values, $g_j(z)$ was approximated by a linear function within each integration interval and inserted into Eq. 20 (or 21) which was then solved for $V_{m,I}$ (or $\Delta V_{m,l}$) to give $i_{m,I}$ (or $i_{m,l}$).

Two complicating factors become evident from the equivalent circuits in Fig. 3: (*a*) the local circuit currents vary with the membrane potential distribution, i.e., with the strength of applied current I. This is a consequence of the dependence of the membrane resistance (r_m) on the membrane potential distribution. (*b*) For the same reason, the fractional shunt current, i.e., the fraction of externally applied current ($i_{e,l}/I$) which flows extracellularly is not constant (at a given position) but depends on the membrane potential (see Fig. 3 *B*).

Numerical Values for Parameters

In working out the distribution of currents and potentials it is necessary to choose numerical data appropriate for a particular preparation. We have used here those applicable for a bundle from frog atrium (100 μm Diam), not only because bundles of this kind are being used in voltage-clamp experiments (see Rougier et al., 1968; Brown and Noble, 1969; Haas et al., 1970; Connor et al., 1975; de Hemptinne, 1976) but also because the physiological properties of these bundles allow the application of the simplifying assumptions discussed in the preceding section. Furthermore, some of the histological and electrical data required were obtained in previous experiments (Lammel et al., 1975), some of which are still unpublished. The following values were used. (See Glossary for definition of symbols.) $a = 4 \cdot 10^{-4}$ cm; $d = 10^{-2}$ cm; $\rho = 0.27$ (Lammel et al., 1975); $c_{K,i}$ and $c_{Na,i} = 150$ and 7.5 mmol/liter, respectively (Keenan and Niedergerke, 1967); $c_{K,R}$ and $c_{Na,R} = 2.5$ and 116.5 mmol/liter, respectively; $G_i = 0.0025\ \Omega^{-1}\ cm^{-1}$ (estimated from unpublished data of Lammel et al. and Weidmann, 1970); $G_R = 0.0125\ \Omega^{-1}\ cm^{-1}$; $P_K = 10^{-6}$ cm s^{-1}, a constant for the case of the unmodified constant-field Eq. 9, otherwise Eq. 10 where it is the P_K value at $V_m = -82$ mV (chosen on the basis of determinations of the membrane conductance at the resting potential in frog atrial trabeculae [Lammel et al., unpublished observations]); $P_{Na} = 0.01 \cdot 10^{-6}$ cm s^{-1} (with $P_{Na}/P_K = 0.01$, see Hodgkin and Horowicz, 1959); $r_i = 7 \cdot 10^6\ \Omega\ cm^{-1}$ (calculated from G_i for the geometrical dimensions of the model trabecula); $T = 293$ K; u_K, u_{Na}, $u_{Cl} = 7.64$, 5.2, and $7.91 \cdot 10^{-4}$ cm^2 s^{-1} V^{-1}, respectively (Conway, 1952; p. 374).

Integration Procedure

Numerical integration of Eqs. 8, 20, and 21 was performed by an extrapolation method based on the midpoint-rule including automatic stepsize correction (Bulirsch and Stoer, 1966). The standard method was adapted to the present purpose and carried out on a TR 440 (Computerbau GmbH, Konstanz, West Germany) computer. Solutions required are determined by (*a*) the condition $i_i = 0$ at both ends of the model trabecula (boundary condition) which describes the fact that the end of a cut or damaged fiber is terminated by a high resistance seal (due to "healing over", Délèze, 1970) and (*b*) continuity conditions for V_m and i_i at the points of transition between the sucrose and the electrolyte compartments ($z = a$ and $z = b$ in Fig. 1). By means of Eq. 6 the conditions for i_i were expressed in terms of dV_m/dz and satisfied within the computation procedure.

RESULTS

The immediate result obtained by integrating Eq. 8 for a given set of conditions is the membrane potential distribution along the model trabecula, from which the current distribution can be calculated by means of the particular I/V relation used. In Figs. 4 and 5 membrane potentials and currents are plotted against distance (z) along three contiguous segments of the bundle, where segment 1, 0.2-mm long, is taken to reside in Ringer's fluid; segment 2, 0.4 or 0.8 mm, in isotonic sucrose and segment 3, 0.4 mm, in isotonic KCl solution. Segmental lengths were chosen on the following grounds: that of segment 1, which is twice the

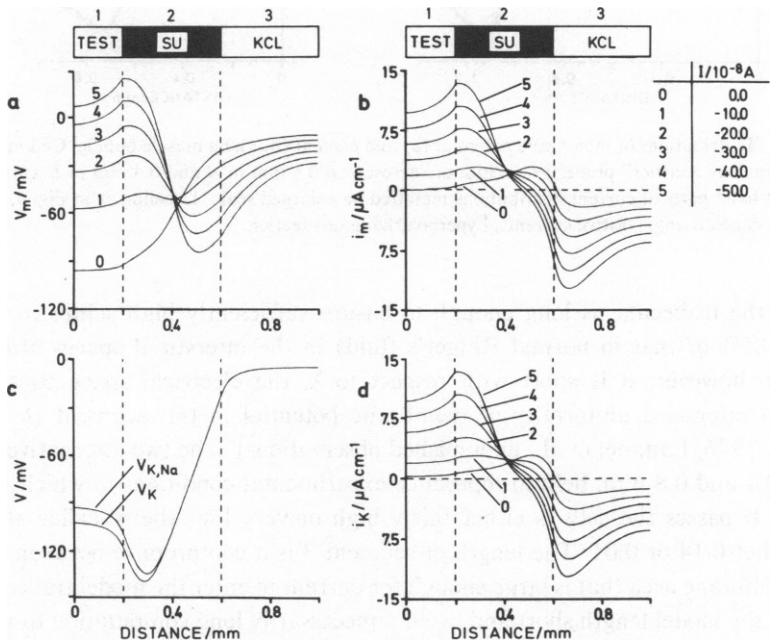

FIGURE 4 Computed distributions of membrane potential (V_m) and current (i_m) along model trabecula under a sucrose gap condition. Lengths of preparation segments and bathing fluids in the three compartments are as indicated. Membrane current (sum of sodium and potassium current [i_K] is assumed to follow the constant field theory [$P_K = 10^{-6}$ cm s^{-1}, $P_{Na}/P_K = 0.01$]). Different profiles correspond to different strengths of applied current (I), given in the table. V_K: potassium equilibrium potential, $V_{K,Na}$: "mixed" equilibrium potential (cf. Eq. 22).

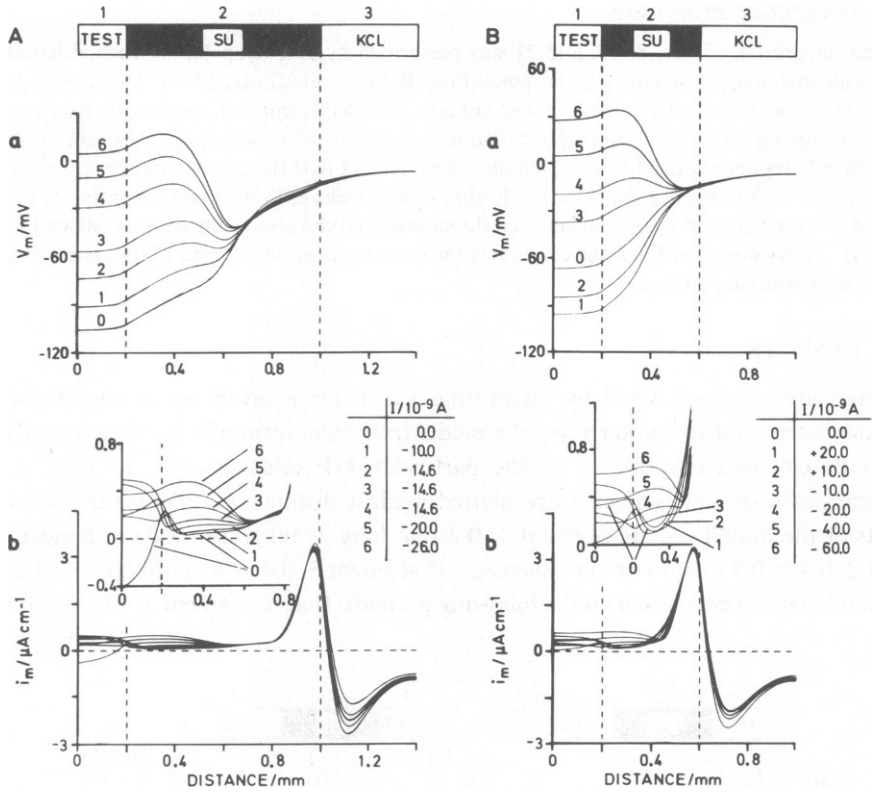

FIGURE 5 Distributions of membrane potential (*a*) and current (*b*) along muscle bundle. Cell membrane with "anomalous rectifier" properties. Width of sucrose gap 0.8 mm in *A* and 0.4 mm in *B* as indicated. *Insets:* left-hand parts of current distributions replotted on enlarged scale. Labeling as in Fig. 4; negative currents *I*, depolarizing; positive currents, hyperpolarizing test section.

diameter of the trabecula, is long enough to ensure sufficiently high solute concentrations (average of 85% of that in normal Ringer's fluid) in the interstitial spaces after diffusion equilibration; however, it is short with respect to λ, the electrical space constant of the trabecula, to safeguard uniformity of membrane potential in this segment ($\lambda \geq 0.6$ mm, Brown et al., 1976; Lammel et al., unpublished observations). The two alternative lengths for segment 2, 0.4 and 0.8 mm, help to reproduce experimental conditions in which the "shunt" current that bypasses the cells is either fairly high or very low, the so-called shunt factor, R_i/R_e, is either 0.14 or 0.01. The length of segment 3 is a compromise between the need to provide a membrane area that is large enough for current to enter the model trabecula and the need to keep the model length short and avoid unnecessarily long computation times.

The results of Figs. 4 and 5 are best discussed together; those of Fig. 4, where the membrane of the model had "classic" constant-field properties ($i_m = i_K + i_{Na}$ given by Eq. 9a,b with P_K and P_{Na} constant), help us to understand the more complex results of main interest (Fig. 5) which were obtained by describing the inward rectifier properties of the cell membrane by Eq. 10. Considering first the computed membrane potentials of Figs. 4*a*, 5*Aa*

and 5*Ba*, it is seen that in the absence of applied current I (curves 0), potentials are low in segment 1 ("resting" potentials), gradually rise through segment 2, and asymptotically approximate the levels set by the equilibrium potential in the high potassium medium (−5 mV) in segment 3. In the presence of applied current I (curves 1–5 of Fig. 4 and curves 1–6 of Figs. 5*Aa* and 5*Ba*), potential profiles show the expected shifts, in the upward (depolarizing) or downward (repolarizing) direction, for increasing outward and inward membrane currents, respectively. As may be noted, these shifts, which occur in both segment 1 and segment 3, extend far into the adjoining regions of section 2 at either end. It is also seen that the results of Figs. 4 and 5 differ in that potential shifts are considerable in both segments 1 and 3 of Fig. 4 and also in segment 1 of Fig. 5, but are quite small in segment 3 of Fig. 5. This illustrates the different rectifier properties introduced: a weak outward rectifier in Fig. 4 and a strong inward rectifier in Fig. 5 (note also the lower current strength required for a given depolarization of segment 1 in Fig. 5 compared with that of Fig. 4).

The families of curves just described have in common that the potential level of each curve is flat enough within segment 1 to allow I/V data to be collected relating the current I to the potential at, say, distance 0.1 mm, the midpoint of this segment. This corresponds to the procedure for determining I/V data experimentally and yields curve 2 of Fig. 6 *A* and the two curves 2 and 3 of Fig. 6 *B*, respectively (output curves). (Current values I were converted into current densities by dividing them by the total membrane area exposed to the test compartment.) These curves clearly resemble the original (input) I/V curves which are also shown in Fig. 6 (curve 1 in both Fig. 6*A* and 6*B*). However, differences are also apparent: for example, compared with curve 1 in Fig. 6 *B*, curve 2 is shifted upwards and much flattened, whereas curve 3 is tilted, right side up and left side down, as well as flattened. The purpose of the subsequent discussion is to elucidate the origin of these modifications, which are attributable to the presence of the sucrose compartment.

To this end, it is best to consider first the membrane current profiles of Fig. 4b and d, which, unlike those of Figs. 5*A*b and 5*B*b, are distinct and readily comparable with the potential profiles in Fig. 4a.

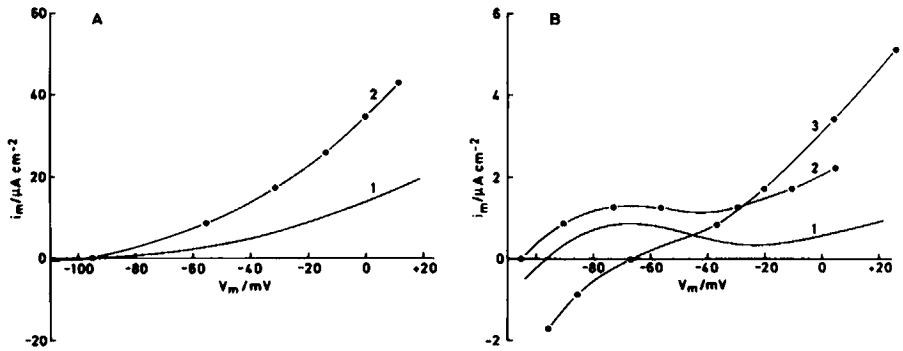

FIGURE 6 Modification of current/voltage curves. (*A*) evaluation of Fig. 4; curve 1, input curve (sum of Eqs. 9a and b with $P_K = 10^{-6}$ cm s^{-1} and $P_{Na} = 10^{-8}$ cm s^{-1}); curve 2, output curve constructed as described in text. (*B*) evaluation of Fig. 5; curve 1, input curve (sum of Eqs. 9a and b with P_K according to Eq. 10 and $P_{Na} = 10^{-8}$ cm s^{-1}); curves 2 and 3, output curves obtained from Fig. 5*A* and 5*B*, respectively.

Three points of main interest are: (*1*) In accordance with the input I/V relation used (sum of Eqs. 9a,b with $P_{Na}/P_K = 0.01$), currents are predominantly carried by potassium ions, as the comparison of Figs. 4*b* and *d*, of the total and potassium currents, respectively, shows.

(*2*) Currents are discernible even under the condition that no external current is applied. These currents, purely of local circuit origin, are most marked at either side of the sucrose-KCl partition because here the gradient of the potassium equilibrium potential along the model trabecula is large (cf. Fig. 4*c*) and the potassium conductance high. The relevance of these currents may be pointed out by noting that in the absence of local current flow (and $I = 0$) the membrane potential at any point along the model trabecula should equal the "mixed" equilibrium potential, $V_{K,Na}$, which, in the present case, is given by

$$V_{K,Na} = \ln \frac{RT}{F} \frac{P_K c_{K,o} + P_{Na} c_{Na,o}}{P_K c_{K,i} + P_{Na} c_{Na,i}}. \tag{22}$$

Levels of this hypothetical potential are illustrated in Fig. 4*c* with those of V_K, the potassium equilibrium potential. The distribution of these two curves is determined by the spatial change of the external potassium and sodium concentrations (cf. Lammel, 1981; Fig. 6*B* for the appropriate concentration profiles).

(*3*) With increasing current I, substantial outward current emerges from the left part of segment 2, the strength of which, close to the 1-2 partition, is even greater than that of the current in segment 1. The explanation is as follows. As is seen in Fig. 4*c* the equilibrium potential for potassium current moves to high negative values in this region, whereas the membrane potential is shifted in the opposite direction (Fig. 4*a*). The driving force for potassium current thereby becomes so large that it more than counterbalances the effect of the reduced potassium conductance at the low level of $c_{K,o}$ in this region.

With regard to the results of Figs. 5*A*b and *B*b, comparison of curves at zero current I (curves 0 in both 5*A*b and 5*B*b) with all others shows that all current profiles are dominated by large components of local current which, as in Fig. 4b, are most striking at either side of the 2-3 partition. Nevertheless, it can be seen in spite of this complication, that considerable outward current crosses the cell membrane in segment 2, when applied current is large (see curves of insets of 5*A*b and *B*b). A further striking feature is the spatial inhomogeneity of some current distributions by comparison with the corresponding membrane potential profiles in the vicinity of the Ringer-sucrose junction. This is an effect due to the extracellular concentration change in this region, since each concentration level is related to a different I/V relationship (see Fig. 2*B*).

For further analysis of the modification of the I/V curves illustrated in Fig. 6 a separation of the currents into those of external and of local circuit origin was performed for the results of Fig. 5*A* and *B* along the lines discussed in connection with Eqs. 20 and 21. The membrane current (i_m) and its two constituent components ($i_{m,I}$ and $i_{m,l}$) were then integrated with respect to length (z) over two regions: (*a*) the length of segment 1 ($0 \leq z \leq 0.2$ mm), and (*b*) the region of current exit ($i_{m,l}$) in segment 2 ($0.2 \leq z \leq 0.76$ mm and $0.2 \leq z \leq 0.46$ mm, respectively). The aim was to convert current densities into currents (I_m, $I_{m,I}$, $I_{m,l}$) for comparison with the currents determined experimentally. The results obtained for the conditions of Fig. 5*A* are illustrated in Fig. 7*A*, those for the conditions of Fig. 5*B* in Fig. 7*B*. In both cases the top panel shows the different currents computed for the test section and the

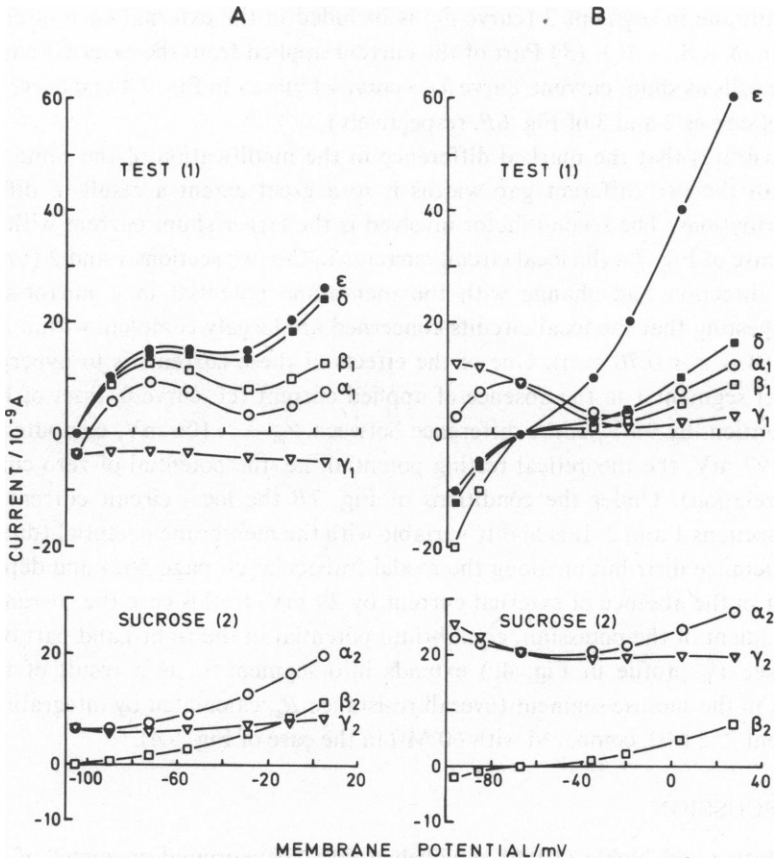

FIGURE 7 Current components of test compartment (top, 1) and of adjoining region of sucrose compartment (bottom, 2). *A*, gap width 0.8 mm; B, gap width 0.4 mm. Membrane current (○) in each of the two compartments (α_1 and α_2, respectively) is composed of current from external current source (□; β_1 and β_2, respectively) and local circuit current (▽; γ_1 and γ_2, respectively): $\alpha_1 = \beta_1 + \gamma_1$; $\alpha_2 = \beta_2 + \gamma_2$. Currents obtained by integration as described in the text and plotted against membrane potential in test compartment. Curve δ (■) in each top panel: sum of currents from external source from test and sucrose region ($\delta = \beta_1 + \beta_2$); curve ϵ (●): measured current, i.e. curve δ plus shunt current.

bottom panel the currents of the adjoining sucrose region plotted against the membrane potential of the test section (at $z = 0.1$ mm). It is important to point out that current I_m (the total current) across the membrane segment 1 (curve α_1 in both Fig. 7*A* and *B*), expressed per unit of membrane surface, is closely similar in magnitude and voltage dependence to the input current of the original I/V curve (at $c_{K,o} = 2.5$ mmol/liter). This follows from the approximate constancy, at different currents I, of both membrane potential and the level of $c_{K,o}$ within this segment, i.e. of the two parameters determining the membrane current according to Eqs. 9 and 10. Modifications of the output I/V relation with regard to this curve are due to the following effects.

(*1*) Since $I_{m,l} = I_m - I_{m,1}$, the current component at each membrane potential which passes from segment 1 into the external circuit (curve β_1) differs from I_m (curve α_1) by the amount of local circuit current of this section (curve γ_1): curve $\alpha_1 \rightarrow$ curve β_1. (*2*) Current which passes

the cell membrane in segment 2 (curve β_2) is included in the external current circuit: curve $\beta_1 \rightarrow$ curve δ ($\delta = \beta_1 + \beta_2$). (*3*) Part of the current applied from the external current source bypasses the cells as shunt current: curve $\delta \rightarrow$ curve ϵ (curve ϵ in Fig. 7*A* and curve ϵ in Fig. 7*B* are replots of curves 2 and 3 of Fig. 6*B*, respectively).

Fig. 7 illustrates that the marked difference in the modification of the same input curve obtained with the two different gap widths is to a great extent a result of different local current distributions. The second factor involved is the larger shunt current with the shorter gap. In the case of Fig. 7*A* the local circuit currents in the two sections 1 and 2 (γ_1 and γ_2) are of opposite direction and change with the membrane potential in a mirror-symmetrical fashion, suggesting that the local circuits concerned are largely complete within the limits of integration ($0 \leq z \leq 0.76$ mm). One of the effects of these currents is to hyperpolarize the membrane of segment 1 in the absence of applied current (cf. curve 0, inset of Fig. 5*A*; the hyperpolarization, by 9mV, is the difference between $V_m = -106$ mV, computed at $z = 0.1$ mm, and -97 mV, the theoretical resting potential, i.e. the potential of zero current of the input I/V relation). Under the conditions of Fig. 7*B* the local circuit current is directed outward in sections 1 and 2. It is highly variable with the membrane potential (due to changes of the conductance distribution along the model trabecula, cf. page 562) and depolarizes the test segment in the absence of external current by 29 mV. In this case the current caused by the large gradient of the potassium equilibrium potential in the right-hand part of the model trabecula (see V_K profile in Fig. 4*c*) extends into segment 1, as a result of the reduced resistance r_e in the sucrose segment (overall resistance R_e, calculated by integration of Eq. 13 along segment 2: 2 MΩ, compared with 60 MΩ in the case of Fig. 5*A*).

DISCUSSION

Although Hutter and Noble (1960) established that "background currents" of cardiac cell membranes resemble those of skeletal muscle fibers in showing the characteristic voltage dependence of the inward rectifier for potassium current, nevertheless both the size and voltage dependence of these currents are, as yet, not well known. There are several reasons for this, including variations and differences in membrane properties from one preparation to the next, especially in preparations taken from different species, as a recent comparative study suggests (Trautwein and McDonald, 1978). The present study shows that an additional and probably important element of uncertainty exists in several distorting effects which are introduced by the sucrose gap method. Figs. 8*A* and *B* summarize once more these distortions for the two variants of the model analyzed, in which the insulating resistance formed by the sucrose gap was taken to be either very high (Fig. 8*A*) or sufficiently low (Fig. 8*B*), so as to simulate an "ideal" experimental condition as well as a rather less favorable one. The differences between the input and output curves shown (cf. curves 1 and 2 in Figs. 8*A* and *B*) are of multiple origin, related to (*a*) local circuit currents due to electromotive forces within the preparation, (*b*) currents which are collected from the membrane of parts of the preparation residing in the sucrose gap and (*c*) shunt currents which bypass the fibers altogether. All these current components alter with the varying strength of the applied current I in a nonlinear fashion.

The two model variants were also used to examine some further conditions of relevance for actual experiments: (*1*) Since, as mentioned on page 560, the flow of local circuit current is

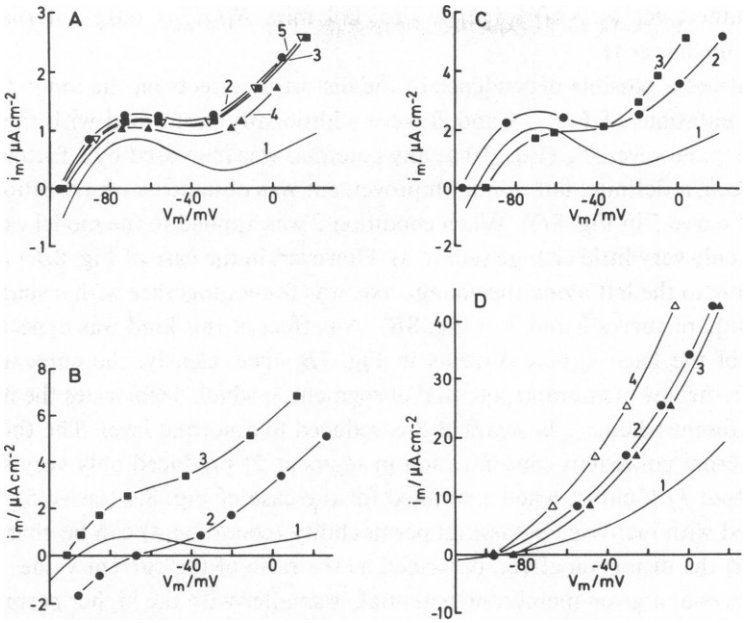

FIGURE 8 Input and output I/V relations for different conditions. Input curve in each panel labeled by 1. Output curves constructed as in Fig. 6. *A-C*, membrane with inward rectifier properties. *D*, constant-field membrane. (*A*)2, replot of curve 2 of Fig. 6*B* (gap width 0.8 mm). Modifications with respect to 2: 3, segment 3 of model trabecula bathed in Ringer's fluid; 4, liquid junction potential absent; 5, external potassium concentration along segment 2 elevated ($c_{K,o} \geq 0.2$ mmol/liter). (*B*)2, replot of curve 3 of Fig. 6*B* (gap width 0.4 mm). Modification with respect to 2: 3, segment 3 bathed in Ringer's fluid. (*C*) modification of input curve (1) with respect to *A* and *B* (permeability increased twofold); 2, gap width 0.8 mm (as in *A*); 3, gap width 0.4 mm (as in *B*). (*D*)2, replot of curve 2 of Fig. 6*A*. Modifications with respect to 2: 3, liquid junction potential absent; 4, double sucrose gap (width of either gap 0.4 mm, node width 0.2 mm). Different conditions for computation of curves in each panel are indicated by both numbering different symbols.

caused (*a*) by the spatial variation of the ionic equilibrium potentials along the trabecula and (*b*) the liquid junction potential in the external fluid, it may be asked to what extent the liquid junction potential contributes to the modification of the I/V curve. This is of interest since effects due to the liquid junction potential have been said to be reduced by placing tight-fitting seals around the preparation between test and sucrose segment (e.g. Stämpfli, 1963; Berger and Barr, 1969). In examining this point, computations were made along the same lines as used in obtaining curve 2 of Fig. 8*A*, but with the term dE_e/dz omitted from Eq. 8, thus simulating a case in which the liquid junction potential is absent altogether.

(*2*) For another set of computations, segment 3 was taken to be surrounded by Ringer's fluid instead of by isotonic KCl, so examining the alternative use of the two fluids in certain experiments (cf. Beeler and Reuter, 1970; Reuter and Scholz, 1977).

(*3*) Contamination of the sucrose solution in segment 2 with potassium ions leaking from the cells (as discussed by Johnson and Lieberman, 1971) was simulated by introducing an analytical expression for the potassium profile into the calculations, which limits the minimum concentration within this region to 0.2 mmol/liter. The effect of this modification consists in a different distribution of V_K along the model trabecula and a decrease of the

external resistance, R_e, by ~50% (gap width: 0.8 mm, R_i/R_e = 0.02, internal resistance assumed to be unchanged).

(*4*) To illustrate a possible dependence of the distorting effects on the input I/V relation, itself, the computations of Fig. 5*A* and *B* were additionally performed with the same input relation in which, however, P_K (Eq. 10) at any potential was increased by a factor of two.

As can be seen, a definite, but minor, improvement was obtained with condition *1* (curve 4 in Fig. 8*A* and curve 3 in Fig. 8*D*). When condition *2* was applied to the model variant of Fig. 8*A*, there was only very little change (curve 3). However, in the case of Fig. 8*B* a marked shift of the I/V curve to the left along the voltage axis was found, together with a shape change of this curve (compare curves 2 and 3 in Fig. 8*B*). An effect of this kind was expected from the consideration of the local circuit currents in Fig. 7*B* since, clearly, the current component associated with the low membrane potential of segment 3, which depolarizes the membrane of segment 1, is absent when $c_{K,o}$ in segment 3 is reduced to a normal level. The third condition (increased external potassium concentration in segment 2) produced only very small alteration of the output I/V curve, when examined for the case of Fig. 8*A* (curve 5). Finally, the results obtained with increased potassium permeability (condition *4*) can be characterized by stating that (*a*) the distortion effect, described as the ratio of the current values of the input and output curves at a given membrane potential, is smaller with the higher permeability (the ratio at $V_m = -40$ mV obtained from curves 1 and 2 in Fig. 8*A* and *C*, being 0.41 and 0.54, respectively), and (*b*) changes of the output curve associated with the different recording conditions of Fig. 5*A* and *B* are less pronounced in this case (compare difference between curves 2 in Fig. 8*A* and *B* with difference between curves 2 and 3 in Fig. 8*C*).

Since the two sets of results of Figs. 8*A* and *B* presumably illustrate extreme experimental situations, it seems justified to discuss a variety of experimental data in the light of the present analysis. However, it should be remembered that the presence of partitions of considerable widths between preparation segments in some experiments and of a second sucrose compartment in others (using the so-called double sucrose gap technique) is expected to result in an increased complexity of the recording situation. In both cases additional membrane areas with properties different from those under examination are present, and a comparison of curves 2 and 4 in Fig. 8*D* provides an example of the additional distorting effect which arises in one of these cases (the case here is the double sucrose gap situation worked out for the model containing the constant field membrane, see legend).

That experimentally recorded I/V curves are modified to extents ranging between the examples given in Fig. 8*A* and *B* is suggested on the following grounds. It seems probable that even tight seals cannot entirely prevent solute transfer from the saline compartments into the sucrose and so keep the external fesistance of segment 2 at the desired high level. In agreement with this, (*a*) resting potentials are usually reduced, if only slightly, after the preparation is placed in the sucrose gap apparatus (though increased potentials have also been recorded, e.g. Connor et al., 1975); (*b*) measured shunt factors are not usually very small but extend within the range <0.1–0.3 (e.g. New and Trautwein, 1972; Goldman and Morad, 1977b; Reuter and Scholz, 1977). With regard to the fact that these shunt factors are often used to characterize an experimental sucrose gap arrangement, computed resting potentials obtained under different conditions are plotted against the respective values of R_i/R_e in Fig. 9. The relationship illustrated by curve 1 is obtained when R_i/R_e is altered by varying the width

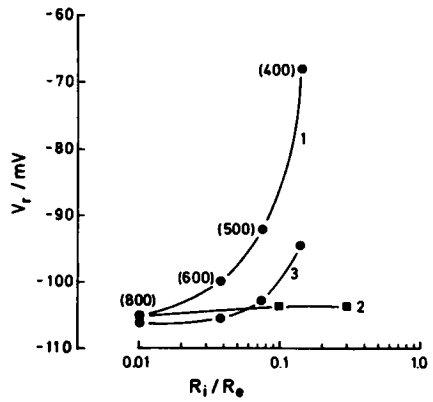

FIGURE 9 Dependence of computed resting potential (V_r) on shunt factor (R_i/R_e). Variations of R_i/R_e either by variation of gap width (●; curves 1 and 3, widths in μm given in brackets), or by variation of R_i only (■; curve 2, gap width 800 μm). 1 and 2: potassium permeability (P_K) as described by Eq. 10; 3: P_K increased twofold.

of the sucrose segment. On the basis of this curve, appreciable membrane depolarization, by 20 mV and more, is expected to occur when R_i/R_e is >0.1, as seems to be the case in many experiments. (The theoretical resting potential in the case of curve 1 is −97 mV.) Although, occasionally, low resting potentials are reported (e.g. a level of −65 mV in Fig. 1 of Goldman and Morad, 1977*a*) potentials do not normally appear to decline below levels of about −75 mV (Goldman and Morad, 1977*a*; Trautwein and McDonald, 1978; Reuter and Scholz, 1977). Two reasons can be adduced from the results additionally included in Fig. 9 to explain this. (*a*) As is known (New and Trautwein, 1972) ratios R_i/R_e increase in the course of

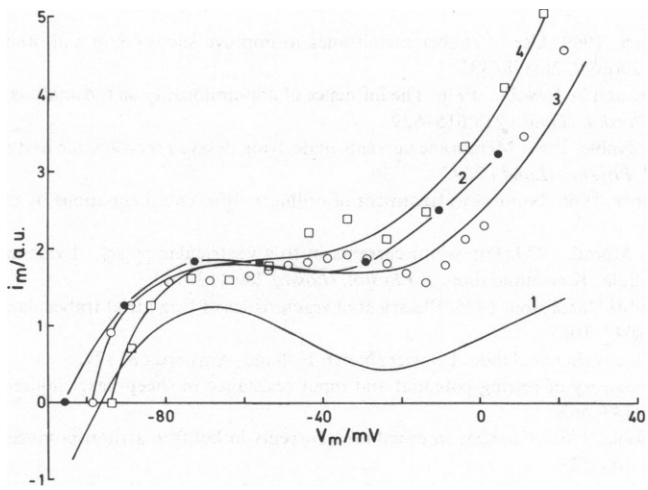

FIGURE 10 Comparison of input curve 1 and output curve 2(●) of Fig. 6*B* with experimentally determined curves of background current (3: eyefit of O; 4: eyefit of □) from Giles and Noble (1976), the latter shifted by 13.9 mV to the left along the voltage axis and scaled to give approximate amplitude fit with curve 2 (see text). All currents in arbitrary units.

sucrose gap experiments because of an increase in R_i. However, a 10-fold, even 30-fold, increase of R_i, at constant R_e, hardly alters the resting potential at all, as the computed potentials of curve 2 in Fig. 9 show. (*b*) If the potassium permeability of the model membrane is taken to be twice as high as that of the initial assumption (compare results of Fig. 9*C*) resting potentials remain within $-107 < V_r < -94$ mV for shunt factors in the range $R_i/R_e <$ 0.14 (R_i/R_e again being changed by variation of the gap width, curve 3, Fig. 9).

Finally, an attempt is made to "correct" experimental I/V data on the basis of the present analysis. For this purpose, data were taken from a preparation with a high resting potential and low factor R_i/R_e, so that the "ideal" situation of Fig. 5*A* can be assumed to have been at least approximated. Fig. 10 shows the plot of two I/V curves from a paper by Giles and Noble (1976) (redrawn from their Figs. 6 and 7; the zero current points of their curves are shifted to the left along the potential axis by 13.9 mV, to allow for the fact that "trans-gap" rather than membrane potentials were recorded and that the level of membrane potential at the partition 2-3 in Fig. 5*A*a of the present paper is -13.9 mV). As is seen, after appropriate scaling, a reasonable fit between experimental and computed data is obtained. One may conclude that the I/V relationship of background currents in frog heart tissue does, most probably, contain a substantial region of negative slope conductance, like that of skeletal muscle (see also Cleemann and Morad, 1979).

I am indebted to Dr. R. Niedergerke, Department of Biophysics, University College London, for much help during the initial, conceptual stages of this work. I would also like to thank Dr. J. F. Hohnsbein, Institut für Arbeitsphysiologie, University of Dortmund, for his valuable comments on the manuscript.

Received for publication 26 August 1980 and in revised form 8 April 1981.

REFERENCES

Beeler, G. W., and H. Reuter. 1970. Voltage clamp experiments on ventricular myocardial fibres. *J. Physiol. (Lond.)* 207:165–190.

Berger, W., and L. Barr. 1969. Use of rubber membranes to improve sucrose-gap and other electrical recording techniques. *J. Appl. Physiol.* 26:378–382.

Brown, H. F., D. Noble, and S. J. Noble. 1976. The influence of non-uniformity on the analysis of potassium currents in heart muscle. *J. Physiol. (Lond.)* 258:615–629.

Brown, H. F., and S. J. Noble. 1969. Membrane currents underlying delayed rectification and pace-maker activity in frog atrial muscle. *J. Physiol. (Lond.)* 204:717–736.

Bulirsch, R., and J. Stoer. 1966. Numerical treatment of ordinary differential equations by extrapolation methods. *Num. Math.* 8:1–13.

Cleemann, L., and M. Morad. 1979. Potassium currents in frog ventricular muscle: Evidence from voltage clamp currents and extracellular K accumulation. *J. Physiol. (Lond.)* 286:113–143.

Connor, J., L. Barr, and E. Jacobsson. 1975. Electrical characteristics of frog atrial trabeculae in the double sucrose gap. *Biophys. J.* 15:1047–1067.

Conway, B. E. 1952. Electrochemical data. Elsevier/North-Holland, Amsterdam. 374.

Délèze, J. 1970. The recovery of resting potential and input resistance in sheep heart injured by knife or laser. *J. Physiol. (Lond.)* 208:547–562.

Giles, W., and S. J. Noble. 1976. Changes in membrane currents in bullfrog atrium produced by acetylcholine. *J. Physiol. (Lond.)* 261:103–123.

Goldman, D. E. 1943. Potential, impedance and rectification in membranes. *J. Gen. Physiol.* 27:37–60.

Goldman, Y., and M. Morad. 1977*a*. Regenerative repolarization of the frog ventricular action potential: A time and voltage-dependent phenomenon. *J. Physiol. (Lond.)* 268:575–611.

Goldman, Y., and M. Morad. 1977*b*. Measurement of transmembrane potential and current in cardiac muscle: A new voltage clamp method. *J. Physiol. (Lond.)* 268:613–654.

Haas, H. G., R. Kern, and H. M. Einwächter. 1970. Electrical activity and metabolism in cardiac tissue: An experimental and theoretical study. *J. Membr. Biol.* 3:180–209.

de Hemptinne, A. 1976. Voltage clamp analysis in isolated cardiac fibres as performed with two different perfusion chambers for double sucrose gap. *Pflügers Arch. Eur. J. Physiol.* 363:87–95.

Hodgkin, A. L., and P. Horowicz. 1959. The influence of potassium and chloride ions on the membrane potential of single muscle fibres. *J. Physiol. (Lond.)* 148:127–160.

Hodgkin, A. L., and B. Katz. 1949. The effect of sodium ions on the electrical activity of the giant axon of the squid. *J. Physiol. (Lond.)* 108:37–77.

Hutter, O. F., and D. Noble. 1960. Rectifying properties of heart muscle. *Nature (Lond.)* 188:495.

Johnson, E. A., and M. Lieberman. 1971. Heart: excitation and contraction. *Annu. Rev. Physiol.* 33:479–532.

Katz, B. 1949. Les constantes électriques de la membrane du muscle. *Arch. Sci. Physiol.* 3:285–300.

Keenan, M. J., and R. Niedergerke. 1967. Intracellular sodium concentration and resting sodium fluxes of the frog heart ventricle. *J. Physiol. (Lond.)* 188:235–260.

Kortüm, G. 1957. Lehrbuch der Elektrochemie. Verlag Chemie, Weinheim. 257.

Lammel, E., R. Niedergerke, and S. Page. 1975. Analysis of a rapid twitch facilitation in the frog heart. *Proc. R. Soc. Lond. B.* 189:577–590.

Lammel, E. 1981. A theoretical study on the sucrose gap technique as applied to multicellular muscle preparations: I. Saline-sucrose interdiffusion. *Biophys. J.* 36:533–553.

McGuigan, J. A. S. 1974. Some limitations of the double sucrose gap, and its use in a study of the slow outward current in mammalian ventricular muscle. *J. Physiol. (Lond.)* 240:775–806.

New, W., and W. Trautwein. 1972. Inward membrane currents in mammalian myocardium. *Pflügers Arch. Eur. J. Physiol.* 334:1–23.

Noble, D. 1975. The initiation of the heartbeat. Clarendon Press, Oxford.

Reuter, H., and H. Scholz. 1977. A study of the ion selectivity and the kinetic properties of the calcium dependent slow inward current in mammalian cardiac muscle. *J. Physiol. (Lond.)* 264:17–47.

Rougier, O., G. Vassort, and R. Stämpfli. 1968. Voltage clamp experiments on frog atrial heart muscle fibres with the sucrose gap technique. *Pflügers Arch. Ges. Physiol.* 301:91–108.

Stämpfli, R. 1963. Die doppelte Saccharosetrennwandmethode zur Messung von elektrischen Membraneigenschaften mit extracellulären Elektroden. *Helv. Physiol. Pharmacol. Acta.* 21:189–204.

Trautwein, W., S. W. Kuffler, and C. Edwards. 1956. Changes in membrane characteristics of heart muscle during inhibition. *J. Gen. Physiol.* 40:135–145.

Trautwein, W., and T. F. McDonald. 1978. Current-voltage relations in ventricular muscle preparations from different species. *Pflügers Arch. Eur. J. Physiol.* 374:79–89.

Weidmann, S. 1970. Electrical constants of trabecular muscle from mammalian heart. *J. Physiol. (Lond.)* 210:1041–1054.